Carbon 99 (2016) 118–122

Contents lists available at ScienceDirect

Carbon

journal homepage: www.elsevier.com/locate/carbon

Raman characterization of AB- and ABC-stacked few-layer graphene by interlayer shear modes

Xin Zhang [a, *], Weng-Peng Han [a], Xiao-Fen Qiao [a], Qing-Hai Tan [a], Yu-Fang Wang [b], Jun Zhang [a], Ping-Heng Tan [a]

[a] State Key Laboratory of Superlattices and Microstructures, Institute of Semiconductors, Chinese Academy of Sciences, Beijing 100083, China
[b] Department of Physics, Nankai University, Tianjin 300071, China

ARTICLE INFO

Article history:
Received 6 September 2015
Received in revised form
24 November 2015
Accepted 25 November 2015
Available online 30 November 2015

ABSTRACT

Stacking order of layered materials strongly influences their electronic properties. Bernal (AB) and rhombohedral (ABC) stacking are much common in few-layer graphenes. Here, we found that AB- and ABC-stacked few-layer graphenes can be well distinguished by whether their highest-frequency shear modes are observed or not in the Raman spectra at room temperature. This method can be expanded to Raman characterization of the stacking order in other two-dimensional layered materials.

1. Introduction

Monolayer graphene (1LG) has received intensive interest because of its unique properties [1–5] which provide the impetus for potential applications as electronic and photonic devices. 1LG can be stacked vertically to form N layer graphene (NLG, $N > 2$) with distinctive band structures. For example, 1LG is a zero-gap semimetal [2,3], whereas bilayer graphene (2LG) is a semiconductor with a tunable band gap [6]. The band structure of trilayer graphene (3LG), in fact, strongly depends on the stacking of the individual graphene sheet. Bernal (AB) and Rhombohedral (ABC) stacking orders are much common in the formation of a few-layer graphene (FLG). AB-stacked 3LG (AB-3LG) has an electrical structure of overlapping linear and quadratic bands [7] while that of ABC-stacked 3LG (ABC-3LG) has a cubic dispersion [8]. When an electric field is applied to 3LG, AB-3LG remains metallic at all fields while ABC-3LG behaves in a similar manner to 2LG with a tunable band gap [9]. The ABC-stacked NLG (ABC-NLG, $N > 3$) is predicted to have even lower kinetic energy than 1LG, 2LG and 3LG, which affords an alternative approach to promote Coulomb interaction between carriers [10]. Besides the band structure, AB-stacked NLG (AB-NLG) and ABC-NLG also exhibit different interlayer screening [11], magnetic state [12,13] and spin–orbit coupling [14]. In view of these differences, researches on NLG require a direct, practical and reliable method to characterize their stacking order at room temperature.

The intrinsic difference in symmetry between AB- and ABC-NLG brings us into the frontier of vibration spectroscopy. Although IR spectroscopy provides a mean of identifying stacking order [15], it requires the specialized instrumentation. Raman spectroscopy, on the other hand, has many advantages over IR spectroscopy and yet has been a versatile tool for studying the properties of graphene [16–18]. For example, the D mode which needs disorders for its activation is widely used to characterize the defects [19] and edges [20–22] in 1LG and FLG. The 2D mode, the second order of the D mode, affords a method to characterize the layer number (N) of AB-NLG ($N = 1 \sim 4$) [23]. Previous Raman characterization of AB- and ABC-stacked FLG was mainly based on the distinctive features of the 2D mode [24–26]. However, the differences in the profile of the 2D mode between AB- and ABC-NLG are much complicated and laser-energy-dependent [24,27,26]. Additionally, the 2D mode is difficult to be applied in N characterization of NLG with $N > 4$, and further to identify stacking order of NLG with $N > 4$. There is still a request for direct and applicable method to characterize the stacking order in NLG.

Interlayer vibrations, including shear (C) and layer breathing (LB) vibrational modes, have received intensive researches in FLG [18,27–33] and transitional metal dichalcogenides [34]. The frequencies of C and LB modes can not be easily observed because of their ultra-low-frequency (ULF) beyond the spectroscopy limitations until Tan et al. successfully detected the highest-frequency C modes in AB-NLG ($N = 2 \sim 16$) [28]. In fact, there are $(N - 1)$ C modes and $(N - 1)$ LB modes for both AB- and ABC-NLG, which we indicate as $C_{N,N-j}$ and $LB_{N,N-j}$, with $j = N - 1, N - 2, \ldots, 1,$

* Corresponding author.
E-mail address: zhangxin@semi.ac.cn (X. Zhang).

http://dx.doi.org/10.1016/j.carbon.2015.11.062
0008-6223/

respectively. In this notation [18,33], for a given N, the labels C_{N1} and LB_{N1} are used for the highest frequency C and LB peaks, and the labels $C_{N,N-1}$ and $LB_{N,N-1}$ are used for the lowest frequency C and LB peaks, respectively. The C_{N1} mode is the only C mode thus far observed in AB-stacked FLG at room temperature [28]. The symmetry of AB stacking and weak electron-phonon coupling (EPC) are responsible for the absence of the other C modes in the Raman spectra [28]. Recently, Lui et al. found that the C_{31} mode of ABC-3LG is infrared (IR) active, while the C_{32} mode is Raman (R) active [35]. They observed the C_{32} mode of ABC-3LG at high temperature of about 800 K by laser heating when ABC-3LG was suspended on quartz substrate and the laser power was increased up to ~ 9 mW [35]. The absence of the C_{31} mode of ABC-3LG is because of its Raman inactivity. Therefore, the stacking order can be revealed from the C modes. Now, Si wafer covered with the SiO_2 layer is widely taken as a substrate to support graphene samples on which electronic devices are fabricated. The C mode observation of ABC-3LG by laser heating and sample suspending is not applicable for most samples on SiO_2/Si substrates for the purpose of basic research and device application. Raman activities of the C modes in AB-*N*LG have been discussed by Tan et al. [28], but those in ABC-*N*LG are not yet reported.

Here, we measure the ULF Raman spectra of both AB- and ABC-*N*LG (N = 3, 4, 5, 6) deposited on SiO_2/Si substrates at room temperature by a low laser power of 0.5 mW. We find that the C_{N1} modes can only be observed in AB-*N*LG, but not in ABC-*N*LG at room temperature. The absence of C_{N1} mode in ABC-*N*LG with odd N is because of symmetry limitations, while those with even N is probably attributed to small EPC. This can be utilized as a new method to distinguish the AB and ABC stacking in *N*LG, which will also benefit the stacking order characterization in other layered materials.

2. Experimental

AB- and ABC-*N*LG are produced by mechanical exfoliation and then transferred onto a Si wafer covered by 93-nm or 300-nm SiO_2. The layer number of graphene flakes is determined by optical contrast [36,37] and the intensity ratio between the Si peak from SiO_2/Si substrates underneath graphene flakes and that from bare SiO_2/Si substrates [38]. The stacking order is determined by the different lineshape of the 2D mode for AB- and ABC-*N*LG [26]. Raman measurements are performed by a Jobin-Yvon HR800 Raman system equipped with a liquid nitrogen cooled charge-coupled detector (CCD). The laser excitation wavelength is 633 nm from a He–Ne laser. A typical laser power at samples is less than 0.5 mW to avoid sample heating. The laser plasma lines are removed by using a BragGrate bandpass filter (OptiGrate Corp.) since these lines would appear in the same spectral range as the C peak. The Rayleigh line is suppressed by using three BragGrate notch filters (OptiGrate Corp.) with an optical density 3 and a spectral bandwidth ~5–10 cm^{-1}. This configuration is similar to that used in Ref. [28]. Argon gas is flowed over the sample to remove the low-frequency Raman modes from air. We use a ×100 objective with a numerical aperture (NA) of 0.90. A 1800 lines per mm grating makes each CCD pixel cover ~0.35 cm^{-1} at 633 nm. A spectral resolution ~0.6 cm^{-1} is estimated from the full width at half maximum (FWHM) of the Rayleigh peak at 633 nm.

3. Results and discussions

Fig. 1 (a) presents the optical image of a mechanically-exfoliated 3LG flake, whose layer number was confirmed by the measured and calculated optical contrast (Fig. 1(b)). The optical image suggests the 3LG flake is quite uniform. However, the Raman spectra

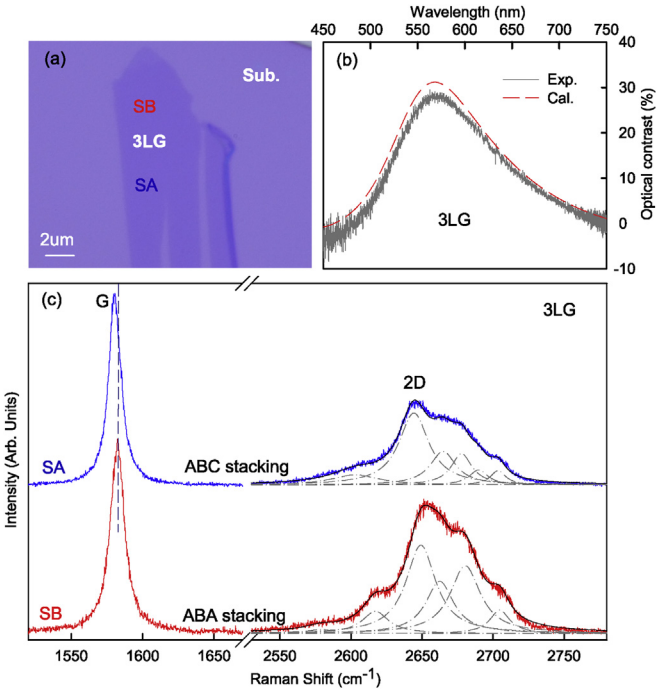

Fig. 1. (a) Optical image of 3LG deposited on the SiO_2/Si substrate. (b) The measured and calculated optical contrast of 3LG. (c) Raman spectra of 3LG measured at two different spots SA and SB, as marked in (a). Dash-dotted lines are the fits to the 2D mode in ABA- and ABC-3LG. (A colour version of this figure can be viewed online).

measured at two spots (SA and SB) in Fig. 1(a) are significantly different. The 2D mode at SB shows an identical spectral profile to a AB-3LG, as shown in Fig. 1(c). The 2D profile in *N*LG reflects its electronic structure [39]. For example, the 2D mode of 1LG is only one Lorentzian peak because Raman scattering for the 2D mode in the visible range is only one process in triple Raman resonance. However, there are two valence and conductance bands in 2LG, where the incident laser can only couple two pairs of these four bands. The two almost degenerate TO phonons in 2LG can couple all electron bands amongst them, which results in four different sub-peaks for the 2D mode [39]. The number of sub-peaks of 2D mode in *N*LG will significantly increase with increasing N [23]. For example, there are fifteen sub-peaks in theory for AB-3LG [40]. Actually, using six sub-peaks can reproduce the profile of 2D mode in AB-3LG [23], as depicted by dash-dotted lines in Fig. 1(c) for the 2D mode at SB. AB-3LG at SB can be further verified by the position of the C mode of AB-3LG in Fig. 2, which will be discussed later. Although the optical contrast of the 3LG flake is quite uniform, the 2D mode at SA exhibits a different spectral profile from that at SB, showing a more asymmetric feature, which is identical to that of ABC-3LG [25,26]. Additionally, the G mode of ABC-3LG (~1581 cm^{-1}) red-shifts compared with AB-3LG (~1582 cm^{-1}), which is attributed to the slight differences between their phonons [25]. The lateral size of the ABC-3LG in Fig. 1(a) around SA is about 4 μm, which can be easily identified from optical images. Mixed ABA and ABC stacking at different area in one graphene flake is very common. Indeed, Lui et al. have found that if the total area associated with the two different stacking orders is considered, ~85% of the area in the samples corresponds to ABA stacking, and ~15% corresponds to ABC stacking [25], which is comparable to that obtained in earlier X-ray diffraction studies of graphite [41].

Similarly, 4-6LG flakes can be firstly identified by optical contrast [36,37] and the Raman mode intensity from Si substrates [38]. Most area of the 4-6LG flakes exhibits the 2D mode of AB-

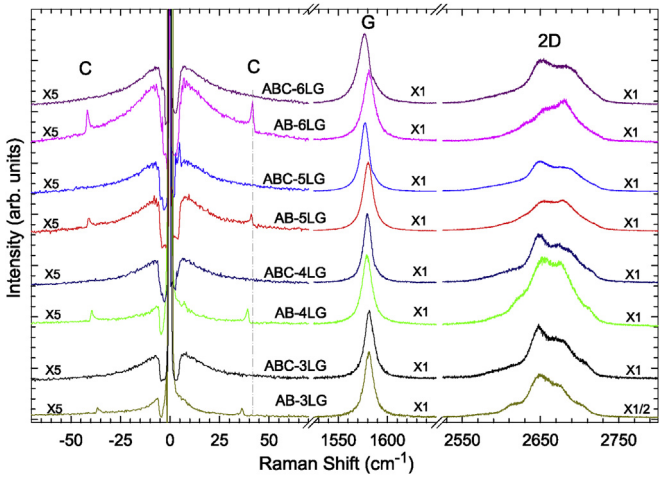

Fig. 2. Raman spectra of AB- and ABC-*N*LG (N = 3, 4, 5, 6) in the C, G and 2D peak spectral regions. The C modes are observed in AB-*N*LG (N = 3, 4, 5, 6), but not in ABC-*N*LG. (A colour version of this figure can be viewed online).

stacked 4–6LG, while a few area exhibits the 2D mode of ABC-stacked 4–6LG, which is similar to the previous reported results [25,26]. The measured Raman spectra of both AB- and ABC-*N*LG (N = 4, 5, 6) are shown in Fig. 2. Fig. S1 in the Supplementary information shows the fits to the 2D mode of AB-4LG and ABC-4LG. Compared with AB-4LG, the red-shifts of the G mode in ABC-4LG is ~1 cm^{-1}, but this value increases up to ~3 cm^{-1} in ABC-5LG and ~5 cm^{-1} in ABC-6LG. The possible reason comes from the N-dependent splitting mediated by the weak interlayer coupling [42].

The main differences between AB- and ABC-*N*LG in the high-frequency region are the peak position of the G mode and the profile of the 2D mode. However, in the ULF region, we can clearly observe the C modes in AB-*N*LG (N = 3, 4, 5, 6) while those in ABC-*N*LG totally disappear, as shown in Fig. 2. These observed C modes are actually the C_{N1} modes [28]. C_{31} mode in AB-3LG lies at ~38 cm^{-1}, which is consistent with our previous results [28]. The C_{31} mode increases into ~40 cm^{-1} (C_{41}) in AB-4LG, ~42 cm^{-1} (C_{51}) in AB-5LG, ~43 cm^{-1} (C_{61}) in AB-6LG and finally reaches at ~44 cm^{-1} in graphite. Besides the observed C_{N1} mode in AB-*N*LG, other C modes are also expected to appear in Raman spectra [28]. For example, the C_{32} mode (~22 cm^{-1}) in AB-3LG, the C_{43} (~17 cm^{-1}) and C_{42} (~31 cm^{-1}) mode in AB-4LG [28]. However, except the C_{N1} mode, other C modes is too weak to be observed as a result of the symmetry limitation or a small EPC [28]. Thus, one reason for the absence of the C_{N1} mode in ABC-*N*LG probably comes from the intrinsic difference in symmetry between AB- and ABC-*N*LG, which makes the C_{N1} mode in ABC-*N*LG Raman-inactive. Another reason is attributed to its small EPC.

The symmetry of the crystal allows us to denote the lattice vibrations, from which we can determine each Raman (R) active vibration. For example, graphite belongs to D_{6h} with its C mode represented by E_{2g}^2, which is R active. The symmetry of AB-*N*LG (N = 2, 3, 4, 5 …) strongly depends on N, which can be divided into D_{3d} for even number of *N*LG (E*N*LG) and D_{3h} for odd number of *N*LG (O*N*LG). There are (N−1) doubly degenerate C modes in *N*LG. As shown in Fig. 3(c) there are two and three C modes expected in AB-3LG and AB-4LG, respectively. Because of their difference in symmetry, the denotations of C modes are significantly different. (N−1) C modes in E*N*LG and O*N*LG are represented by $\frac{N}{2}E_g+\frac{N-2}{2}E_u$ and $\frac{N-1}{2}E''+\frac{N-1}{2}E'$, respectively. E_g and E'' are R active, E_u is Infrared (IR) active, E' is both R and IR active. According to their Raman tensors [43], only E_g and E' can be observed under back-scattering configuration. Symmetry, frequency and normal mode displacement for each C mode of AB-3LG and AB-4LG are depicted in Fig. 3. The C_{N1} mode in AB-stacked E*N*LG (E_g), O*N*LG (E') and graphite (E_{2g}^2) are all R active, which has been experimentally observed [28]. Accordingly, ABC-*N*LG belongs to D_{3d} with their C modes represented by $\frac{N-1}{2}E_g+\frac{N-1}{2}E_u$ for O*N*LG and $\frac{N}{2}E_g+\frac{N-2}{2}E_u$ for E*N*LG. Symmetry, frequency and normal mode displacement for each C mode of ABC-3LG and ABC-4LG are also depicted in Fig. 3. It should be noticed that the C_{N1} mode in ABC-stacked E*N*LG (E_g) is R active, whereas that in ABC-stacked O*N*LG (E_u) is IR active. It suggests that the absence of the C_{N1} mode in ABC-*N*LG (N = 3, 5, 7 …) is the result of their intrinsic difference in symmetry between AB- and ABC-*N*LG. So we expect that AB- and ABC-*N*LG (N = 3, 5, 7 …) can be distinguished by whether their C_{N1} modes are observed or not, as shown in Fig. 2 for 3LG and 5LG. The C_{N1} modes (E_g) in ABC-*N*LG (N = 4, 6, 8 …) are R active, thus, these C modes are expected to appear in Raman spectra as that in AB-*N*LG (N = 4, 6, 8 …). However, we did not observe any C mode in ABC-4LG and ABC-6LG (Fig. 2). The possible reason comes from its small EPC, which is identical to the absence of other C modes except the C_{N1} modes in AB-*N*LG [28]. Because the electronic structure of ABC-*N*LG is different from that of AB-*N*LG, the different EPC strength for the C_{N1} mode compared with that in AB-*N*LG is expected. Thus, the EPC strength should be responsible for the absence of the C_{N1} modes in ABC-*N*LG (N = 4, 6, 8 …), which needs further calculations. The absence of the C_{N1} modes in ABC-*N*LG (N = 3, 4, 5, 6), with the reason either from symmetry limitations in O*N*LG or from EPC in E*N*LG, affords a direct and effective method to characterize the stacking order in *N*LG.

Next, we analysis the optical activities of (N − 1) doubly-degenerated C modes in ABC-*N*LG ($N \geq 3$) based on their vibration displacements obtained from a simple linear-chain model (LCM). LCM has been applied to obtain the dependencies of the frequencies of C modes (ω_C) on N in both FLG [28] and transition metal dichalcogenides [43], where only the nearest interlayer coupling is considered in layered materials. Each graphene layer in *N*LG can be considered as a single atom in LCM, where we do not need to account the stacking order. Thus, we can also apply LCM to ABC-*N*LG. By solving the dynamic matrix, we obtain a general relation between $\omega_C(N)$ and N as follows: $\omega C(N) = \omega C(2)\sqrt{1\pm cos(N_0\pi/N)}$ ($N \geq 2N_0$, N_0 is an integer: 1, 2, 3, 4 … .), where $\omega C(2) = (1/\sqrt{2}\pi c)\sqrt{\alpha/\mu}$ is the C mode frequency in 2LG, $\mu = 7.6 \times 10^{-8}$ g/cm^2 is the mass of one graphene sheet per unit area, c is the speed of light, α~12.8×10^{18} N/m^3 is the interlayer force constant per unite area. As shown in Fig. 4(a), a pair of branches generate from ($2N_0$)LG where the mode frequency of one branch (denoted by $C_{2N_0}^+$) increases with increasing N and that of another branch (denoted by $C_{2N_0}^-$) decreases with increasing N. The modes of the $C_{2N_0}^+$ and $C_{2N_0}^-$ branches are actually the C_{N1} and $C_{N,N-1}$ modes, respectively [18,33]. By solving the dynamic matrix, we also obtained the vibration displacements from which we can determine whether each mode is R active (Fig. 2(c)). The rectangle and triangle in Fig. 4 denote the R and IR active modes, respectively. The optical activity of each C mode in AB-*N*LG has been discussed by Tan et al. [28]. The C_2^+ branch is either R or both R and IR active, while the C_2^- branch is R active. Only the C_2^+ branch is detected in the experiment. The absence of the C_2^- branch was attributed to its small EPC.

Finally, we mainly focused on the C_2^+ and C_2^- branches in ABC-*N*LG. It should be noted that $\omega_C(2)$ is absent in ABC-*N*LG because at least three layers are required in ABC stacking order. However, we still denote the pair of branches from 2LG by C_2^+ and C_2^- in ABC-*N*LG as that in AB-*N*LG. The C_2^- branch of ABC-*N*LG is R active, but we do not detect any C modes (Fig. 2). Lui et al. recently observed the C_{32} mode (lying in C_2^- branch) in ABC-3LG suspended on quartz substrate at high temperature of about 800 K by increasing the laser power up to ~9 mW [35]. The high laser power will remove the

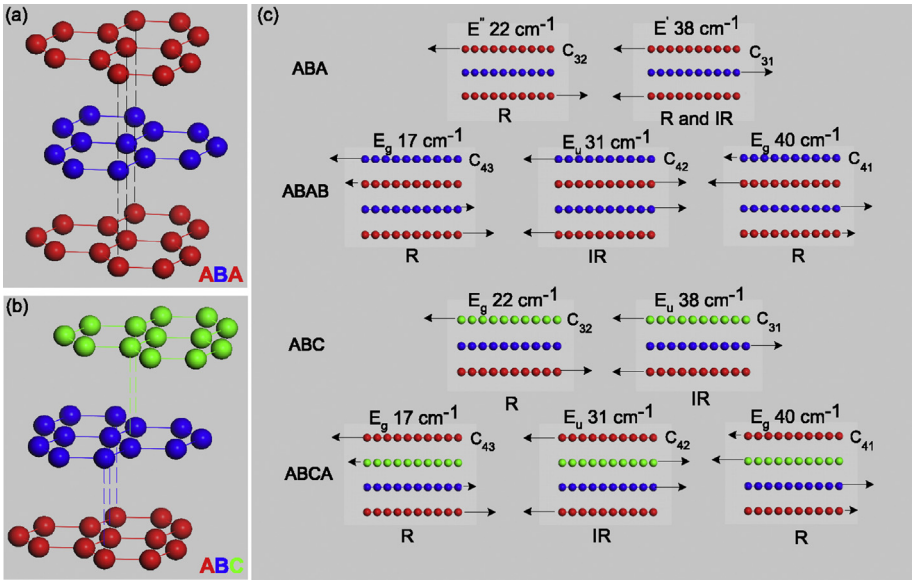

Fig. 3. Schematic illustration of AB-3LG (a) and ABC-3LG (b) in atomic structure. (c) Symmetry, frequency and normal mode displacement for each C mode of AB- and ABC-*N*LG ($N = 3, 4$). The C_{31} mode of AB-3LG is Raman (R) active while that of ABC-3LG is Raman-inactive. The C_{41} modes of AB- and ABC-4LG are both R active. (A colour version of this figure can be viewed online).

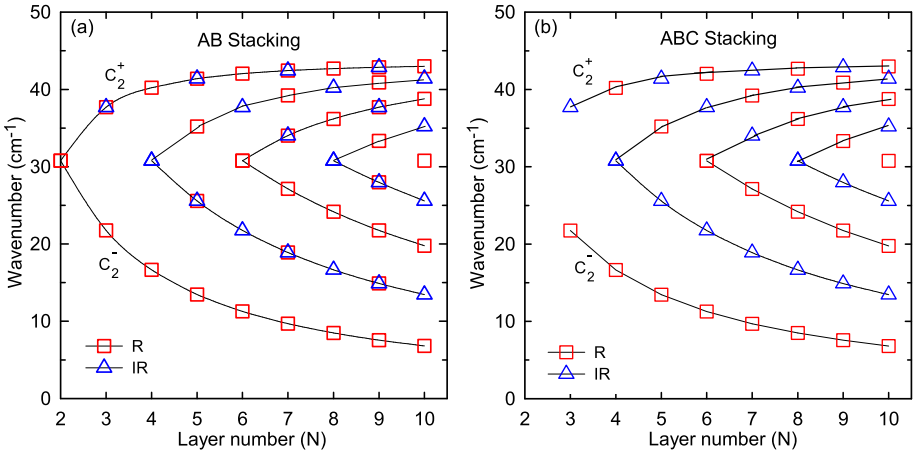

Fig. 4. The frequencies of C modes in *N*LG for AB stacking (a) and ABC stacking (b) as a function of *N*. The rectangles and triangles denote the Raman (R) and infrared (IR) active modes, respectively. C_2^+ and C_2^- denote the pair of branches from 2LG. (A colour version of this figure can be viewed online).

surface adsorbates, which also allows the observation of LB modes in AB-*N*LG [30]. The C_{31} mode in ABC-3LG is absent in their experiments [35] even the laser power was increased up to ~9 mW. This is completely consistent with our results in Fig. 2 because the C_{31} mode is R inactive (Fig. 3(c)).

We measured the ULF Raman spectra of AB-3LG, AB-4LG and AB-5LG which are suspended on Si substrates by increasing the laser power to ~10 mW, but didn't detect any C mode (Supplementary information, Fig. S2) because of the strong background induced by the intense laser power. The C_{32} intensity in ABC-3LG is predicted to be ~0.57 times that of the C_{31} mode in AB-3LG [35], thus, the absence of the C modes in AB-3LG suspended on SiO_2/Si substrates excited by a laser power of ~10 mW suggests that we cannot detect any C mode even if the suspended ABC-3LG on SiO_2/Si substrates is excited by a laser poser of ~10 mW. Recently, Luo et al. predict that the C_{N1} mode in ABC-stacked E*N*LG has a much smaller intensity than the $C_{N,N-1}$ mode [44]. This is consistent with the absence of the C_{N1} mode in ABC-stacked E*N*LG, as shown in Fig. 2. Thus, the absence of the C_{N1} mode in ABC-*N*LG can be utilized to characterize the stacking order in FLG at room temperature.

4. Conclusion

In conclusion, we observed the highest-frequency C modes (C_{N1}) in AB-*N*LG ($N = 3, 4, 5, 6$), but not in ABC-*N*LG. The absence of the C_{N1} mode in ABC-3LG and ABC-5LG results from the symmetry limitations, whereas that in ABC-4LG and ABC-6LG probably comes from the weak electron-phonon coupling. AB- and ABC-*N*LG can be effectively characterized by whether their C_{N1} modes are observed or not at room temperature. This affords a direct and reliable method to distinguish different stacking order in FLG at room temperature. It also benefits the characterization of stacking order in other two-dimensional layered materials.

Acknowledgments

We acknowledge support from the National Natural Science Foundation of China, grants 11225421, 11434010 and 11474277.

Appendix A. Supplementary data

Supplementary data related to this article can be found at http://dx.doi.org/10.1016/j.carbon.2015.11.062.

References

[1] K.S. Novoselov, A.K. Geim, S.V. Morozov, D. Jiang, Y. Zhang, S.V. Dubonos, et al., Electric field effect in atomically thin carbon films, Science 306 (5696) (2004) 666–669.
[2] Y. Zhang, Y. Tan, H. Stormer, P. Kim, Experimental observation of the quantum hall effect and berry's phase in graphene, Nature 438 (7065) (2005) 201–204.
[3] K.S. Novoselov, A.K. Geim, S.V. Morozov, D. Jiang, M.I. Katsnelson, I.V. Grigorieva, et al., Nature 438 (7065) (2005) 197–200.
[4] A.K. Geim, K.S. Novoselov, The rise of graphene, Nat. Mater 6 (3) (2007) 183–191.
[5] F. Bonaccorso, Z. Sun, T. Hasan, A.C. Ferrari, Graphene photonics and optoelectronics, Nat. Photonics 4 (9) (2010) 611–622.
[6] K.S. Novoselov, E. McCann, S.V. Morozov, V.I. Fal'ko, M.I. Katsnelson, U. Zeitler, et al., Unconventional quantum hall effect and berry's phase of 2π in bilayer graphene, Nat. Phys. 2 (3) (2006) 177–180.
[7] T. Taychatanapat, K. Watanabe, T. Taniguchi, P. Jarillo-Herrero, Quantum hall effect and landau-level crossing of dirac fermions in trilayer graphene, Nat. Phys. 7 (8) (2011) 621–625.
[8] F. Zhang, B. Sahu, H. Min, A.H. MacDonald, Band structure of ABC-stacked graphene trilayers, Phys. Rev. B 82 (2010) 035409.
[9] C.H. Lui, Z.Q. Li, K.F. Mak, E. Cappelluti, T.F. Heinz, Observation of an electrically tunable band gap in trilayer graphene, Nat. Phys. 7 (12) (2011) 944–947.
[10] A. Yacoby, Graphene: Tri and tri again, Nat. Phys. 7 (12) (2011) 925–926.
[11] M. Koshino, Interlayer screening effect in graphene multilayers with ABA and ABC stacking, Phys. Rev. B 81 (2010) 125304.
[12] M. Otani, M. Koshino, Y. Takagi, S. Okada, Intrinsic magnetic moment on (0001) surfaces of rhombohedral graphite, Phys. Rev. B 81 (2010) 161403.
[13] M. Otani, Y. Takagi, M. Koshino, S. Okada, Phase control of magnetic state of graphite thin films by electric field, Appl. Phys. Lett. 96 (24) (2010) 242504.
[14] E. McCann, M. Koshino, Spin-orbit coupling and broken spin degeneracy in multilayer graphene, Phys. Rev. B 81 (2010) 241409.
[15] K.F. Mak, J. Shan, T.F. Heinz, Electronic structure of few-layer graphene: Experimental demonstration of strong dependence on stacking sequence, Phys. Rev. Lett. 104 (2010) 176404.
[16] A. Jorio, M.S. Dresselhaus, R. Saito, G. Dresselhaus, Raman Spectroscopy in Graphene Related Systems, Wiley-VCH, 2011.
[17] A.C. Ferrari, D.M. Basko, Raman spectroscopy as a versatile tool for studying the properties of graphene, Nat. Nanotech 8 (4) (2013) 235–246.
[18] J.B. Wu, X. Zhang, M. Ijas, W.P. Han, X.F. Qiao, X.L. Li, et al., Resonant raman spectroscopy of twisted multilayer graphene, Nat. Comm. 5 (2014) 5309.
[19] L.G. Cancado, A. Jorio, E.H.M. Ferreira, F. Stavale, C.A. Achete, R.B. Capaz, et al., Quantifying defects in graphene via raman spectroscopy at different excitation energies, Nano Lett. 11 (8) (2011) 3190–3196.
[20] C. Casiraghi, A. Hartschuh, H. Qian, S. Piscanec, C. Georgi, A. Fasoli, et al., Raman spectroscopy of graphene edges, Nano Lett. 9 (4) (2009) 1433–1441.
[21] X. Zhang, Q.Q. Li, W.P. Han, Y. Lu, W. Shi, J.B. Wu, et al., Raman identification of edge alignment of bilayer graphene down to the nanometer scale, Nanoscale 6 (2014) 7519–7525.
[22] Q.Q. Li, X. Zhang, W.P. Han, Y. Lu, W. Shi, J.B. Wu, et al., Raman spectroscopy at the edges of multilayer graphene, Carbon 85 (2015) 221–224.
[23] W.J. Zhao, P.H. Tan, J. Zhang, J. Liu, Charge transfer and optical phonon mixing in few-layer graphene chemically doped with sulfuric acid, Phys. Rev. B 82 (2010) 245423.
[24] C. Cong, T. Yu, H. Wang, Raman study on the g mode of graphene for determination of edge orientation, ACS Nano 4 (6) (2010) 3175–3180.
[25] C.H. Lui, Z. Li, Z. Chen, P.V. Klimov, L.E. Brus, T.F. Heinz, Imaging stacking order in few-layer graphene, Nano Lett. 11 (1) (2011) 164–169.
[26] T.A. Nguyen, J.U. Lee, D. Yoon, H. Cheong, Excitation energy dependent raman signatures of ABA- and ABC-stacked few-layer graphene, Sci. Rep. 4 (2014) 4630.
[27] C.H. Lui, L.M. Malard, S. Kim, G. Lantz, F.E. Laverge, R. Saito, et al., Observation of layer-breathing mode vibrations in few-layer graphene through combination raman scattering, Nano Lett. 12 (11) (2012) 5539–5544.
[28] P.H. Tan, W.P. Han, W.J. Zhao, Z.H. Wu, K. Chang, H. Wang, et al., The shear mode of multilayer graphene, Nat. Mater 11 (4) (2012) 294–300.
[29] C.H. Lui, T.F. Heinz, Measurement of layer breathing mode vibrations in few-layer graphene, Phys. Rev. B 87 (2013) 121404.
[30] C.H. Lui, Z. Ye, C. Keiser, X. Xiao, R. He, Temperature-activated layer-breathing vibrations in few-layer graphene, Nano Lett. 14 (8) (2014) 4615–4621.
[31] P.H. Tan, J.B. Wu, W.P. Han, W.J. Zhao, X. Zhang, H. Wang, et al., Ultralow-frequency shear modes of 2-4 layer graphene observed in scroll structures at edges, Phys. Rev. B 89 (2014) 235404.
[32] C. Cong, T. Yu, Enhanced ultra-low-frequency interlayer shear modes in folded graphene layers, Nat. Comm. 5 (2014) 4709.
[33] J.B. Wu, Z.X. Hu, X. Zhang, W.P. Han, Y. Lu, W. Shi, et al., Interface coupling in twisted multilayer graphene by resonant raman spectroscopy of layer breathing modes, ACS Nano 9 (7) (2015) 7440–7449.
[34] X. Zhang, X.F. Qiao, W. Shi, J.B. Wu, D.S. Jiang, P.H. Tan, Phonon and raman scattering of two-dimensional transition metal dichalcogenides from monolayer multilayer to bulk material, Chem. Soc. Rev. 44 (2015) 2757.
[35] C.H. Lui, Z. Ye, C. Keiser, E.B. Barros, R. He, Stacking-dependent shear modes in trilayer graphene, Appl. Phys. Lett. 106 (4) (2015) 041904.
[36] P. Blake, E.W. Hill, A.H.C. Neto, K.S. Novoselov, D. Jiang, R. Yang, et al., Making graphene visible, Appl. Phys. Lett. 91 (6) (2007) 063124.
[37] W.P. Han, Y.M. Shi, X.L. Li, S.Q. Luo, Y. Lu, P.H. Tan, The numerical-aperture-dependent optical contrast and thickness determination of ultrathin flakes of two-dimensional atomic crystals: A case of graphene multilayers, Acta Phys. Sin. 62 (2013) 110702.
[38] X.L. Li, X.F. Qiao, W.P. Han, Y. Lu, Q.H. Tan, X.L. Liu, et al., Layer number identification of intrinsic and defective multilayered graphenes up to 100 layers by the raman mode intensity from substrates, Nanoscale 7 (2015) 8135.
[39] A.C. Ferrari, J.C. Meyer, V. Scardaci, C. Casiraghi, M. Lazzeri, F. Mauri, et al., Raman spectrum of graphene and graphene layers, Phys. Rev. Lett. 97 (2006) 187401.
[40] L.M. Malard, M.A. Pimenta, G. Dresselhaus, M.S. Dresselhaus, Raman spectroscopy in graphene, Phys. Rep. 473 (5C6) (2009) 51–87.
[41] H.A. Wilhelm, B. Croset, G. Medjahdi, Proportion and dispersion of rhombohedral sequences in the hexagonal structure of graphite powders, Carbon 45 (12) (2007) 2356–2364.
[42] J.A. Yan, W.Y. Ruan, M.Y. Chou, Phonon dispersions and vibrational properties of monolayer, bilayer, and trilayer graphene: Density-functional perturbation theory, Phys. Rev. B 77 (2008) 125401.
[43] X. Zhang, W.P. Han, J.B. Wu, S. Milana, Y. Lu, Q.Q. Li, et al., Raman spectroscopy of shear and layer breathing modes in multilayer MoS_2, Phys. Rev. B 87 (2013) 115413.
[44] X. Luo, C. Cong, X. Lu, T. Yu, Q. Xiong, S.Y. Quek, Stacking sequence determines Raman intensities of observed interlayer shear modes in 2D layered materials – A general bond polarizability model, Sci. Rep. 5 (2015) 14565.